Catalysis Today 139 (2008) 113–118

Contents lists available at ScienceDirect

Catalysis Today

journal homepage: www.elsevier.com/locate/cattod

Oxygen activation on Cu/Mn–Ce mixed oxides and the role in diesel soot oxidation

Qing Liang, Xiaodong Wu *, Duan Weng, Haibo Xu

Laboratory of Advanced Materials, Department of Materials Science and Engineering, Tsinghua University, Beijing 100084, China

ARTICLE INFO

Article history:
Available online 11 September 2008

Keywords:
Ceria-based oxides
Transitional metals
Oxygen activation
Soot oxidation

ABSTRACT

The Cu- and Mn-doped ceria were prepared using the citric acid sol–gel method. The structural and redox properties of the mixed oxides were investigated by means of XRD, BET, O_2-TPD, CO-TPR and CO reduction under isothermal conditions. TPO tests were performed to evaluate the catalytic activity for soot oxidation. The results showed that Mn^{x+} cations entered into the ceria lattice to form solid solutions, which increased the amount of oxygen vacancies and promoted surface oxygen chemisorption. Cu_xO clusters were more likely to be dispersed on the surface of ceria particles. The interaction between copper and cerium greatly enhanced the rapid release of lattice oxygen of the oxides in the reducing atmosphere. These two mixed oxides showed improved catalytic activities and selectivities to CO_2 for soot oxidation compared with pure ceria. The order of activities under different contact conditions was believed to be related to active oxygen species released by the catalysts.

1. Introduction

CeO_2 has been widely used in automobile exhaust three-way catalysts (TWCs) due to its outstanding oxygen storage capacity (OSC) [1–3]. Ceria-based catalysts recently gain more attention on the utilization for diesel soot oxidation [4–7]. It is presented by Bueno-López et al. [4] through the ^{18}O isotope exchange experiment that the active oxygen on the surface of CeO_2 is a determining factor for soot catalytic oxidation. The temperature of oxygen activation can be lowered ca. 100 °C by the CeO_2 catalyst and thus the combustion rate of soot is increased.

Instead of using ceria alone as the catalyst for diesel soot oxidation, more researchers focus on modification of CeO_2 with different ions to increase the activity and thermal stability. The substitution of Ce^{4+} by Zr^{4+} or La^{3+} favors the creation of structural defects, accelerates oxygen diffusion and induces more surface active oxygen species which further promote the soot oxidation [8–11]. Doping with other rare earth elements (La, Pr, Sm, Y) also improves the activity and stability of ceria due to the increase of meso/macro-pore volume and stabilization of surface area after aging treatment [6]. Compared with rare earth metals, transition metals usually exhibit several oxidation states and better redox properties. Good redox properties and strong interaction between transition metals and ceria make the transition metal–Ce mixed oxides as candidate catalysts for diesel soot oxidation. Recent reports have shown the activity of ceria in complete oxidation reactions can be largely enhanced by transition metals in general. Tikhomirov et al. [12] have found that the incorporation of Mn into the ceria lattice favors the soot oxidation activity of the catalyst. The onset temperature of MnO_x–CeO_2 mixed oxides for the NO-free oxidation lies around 400 °C under loose contact conditions, while that for NO assisted oxidation starts at around 100 °C lower temperature. Our previous studies have also shown that copper modification increases the activity and selectivity of CeO_2. Cu_xO–CeO_2 mixed oxides exhibit the maximum oxidation rate at 496 °C under loose contact conditions for the NO-free oxidation and at 419 °C for NO-assisted oxidation. And this advantage is maintained after aging at 800 °C for 20 h [13,14].

Structural and redox properties of catalysts are always important factors for catalytic reactions. In this paper, the Cu- and Mn-doped CeO_2, which have different morphological states of doping elements and oxygen activation performances, were synthesized by the sol–gel method, and the influence of these structural and redox properties on soot oxidation activities were investigated. As demonstrated by lots of results, the activity of soot catalytic oxidation is mostly influent by the contact mode between soot and catalysts [15,16]. Here, the effect of active oxygen species on the activity of the catalysts under different contact conditions was especially discussed.

2. Experimental

2.1. Catalyst preparation

All the samples were prepared by the sol–gel method. The nitrates $Ce(NO_3)_3{\cdot}6H_2O$ (99.0 wt.%, Beijing Yili) and $Cu(NO_3)_2{\cdot}3H_2O$

* Corresponding author. Tel.: +86 10 62792375; fax: +86 10 62792375.
E-mail address: wuxiaodong@tsinghua.edu.cn (X. Wu).

0920-5861/$ – see front matter © 2008 Elsevier B.V. All rights reserved.
doi:10.1016/j.cattod.2008.08.013

(99.5 wt.%, Yili) were mixed in deionized water according to the molar ratio of Cu:Ce = 1:9. The citric acid was used as the complexing agent with a 1.3:1 ratio of the acid to metal ions including Ce^{3+} and Cu^{2+}. Appropriate polyglycol was followed with the weight of 10% citric acid added. The blended solution was sufficiently mixed in a magnetic stirrer and heated at 80 °C till transparent gel was formed. The resulting gel was dried at 110 °C overnight. The received powders were submitted to decomposition at 300 °C for 1 h and calcination at 500 °C for 3 h under static air in a muffle. The powders were cooled to room temperature (RT) in the furnace to obtain the Cu–Ce mixed oxides. The Mn–Ce mixed oxides (the molar ratio of Mn:Ce = 1:9) and ceria were prepared by the same method with $Mn(NO_3)_2$ (50% water solution, Yili) and $Ce(NO_3)_3{\cdot}6H_2O$ as the precursors.

2.2. Catalyst characterization

The powder X-ray diffraction (XRD) experiments were performed on a Japan Science D/max-RB diffractometer employing Cu Kα radiation (λ = 1.5418 Å). The X-ray tube was operated at 40 kV and 120 mA. The X-ray powder diffractogram was recorded at 0.02° intervals in the range of $20° \leq 2\theta \leq 80°$ with a scanning velocity of 6°/min.

The specific surface areas of the samples were measured using the N_2 adsorption isotherm at −196 °C by the one-point Brunauer–Emmett–Teller (BET) method using an automatic surface analyzer (Quantachrome NOVA 4000). The samples were degassed in flowing N_2 at 200 °C for 2 h.

Temperature programmed desorption (TPD) of O_2 was performed in a fixed-bed reactor with the effluent gases monitored using a quadrupole mass spectrometer (MS) (Omnistar 200). Prior to O_2-TPD experiment, 100 mg sample was treated with O_2 with a total flow rate of 50 ml/min at 500 °C for 30 min, then cooled down to RT under the same atmosphere, and subsequently flushed by 50 ml/min He for 30 min to remove the physisorbed molecules. Finally, the reactor temperature was raised up to 800 °C at a constant heating rate of 10 °C/min. O_2 desorbed during the experiment was simultaneously monitored by MS.

CO temperature programmed reduction (TPR) was performed in a fixed-bed reactor with the effluent gases monitored using a quadrupole MS (Omnistar 200). Prior to CO-TPR experiment, 50 mg sample was treated with O_2 (2 vol%)/He with a total flow rate of 50 ml/min at 500 °C for 30 min, then cooled down to RT in the same atmosphere. It was subsequently flushed by 50 ml/min He for 30 min to remove the physisorbed molecules. Finally, the reactor temperature was raised up to 600 °C at a heating rate of 10 °C/min in CO (4 vol%)/He with a flow rate of 75 ml/min. CO_2 and CO production during the experiment was simultaneously monitored by MS.

CO reduction test was performed in a flow reactor system under isothermal conditions (300, 350, 400, 450 and 500 °C). Typically, 25 mg powders were loaded into a 1.0-cm i.d. quartz tube reactor. The sample was first heated in O_2 for at least 20 min at the desired temperature, purged in He for 10 min to remove oxygen from the system and then exposed constantly to 4% CO/He. A total gas flow rate of 300 ml/min was employed. Instantaneous CO_2 concentration in the outlet gas in the first 50 s was detected by an on-line quadrupole mass spectrometer (Omnistar 200).

2.3. Activity measurement

Printex-U (Degussa) was used a model soot. Its particle size was 25 nm and specific surface was 100 m^2/g. The catalytic activity was evaluated by a temperature programmed oxidation (TPO) reaction apparatus. Before the reaction, the soot–catalyst mixture, in a 1/10 weight ratio, were milled in an agate mortar for "tight contact" or mixed carefully by a spatula for "loose contact". 110 mg catalyst–soot mixture was placed in the tubular quartz reactor (i.d. = 10 mm), and the oxidation test was carried out in the temperature range from RT to 700 °C at a heating rate of 10 °C/min. The inlet gas mixture was 10% O_2 in nitrogen with a flow rate of 500 ml/min. The concentrations of CO_2 and CO in the outlet gases were determined on-line by a five-component analyzer FGA4015 with infrared sensor.

Table 1
The lattice constant and specific surface area of the samples

Samples	Lattice constant (Å)	Crystallite size (Å)	BET surface area (m^2/g)
CeO_2	5.410	78	61.8
Cu–Ce	5.411	59	68.4
Mn–Ce	5.406	47	72.5

3. Results and discussion

3.1. XRD and BET

The XRD patterns of the samples are shown in Fig. 1. All the samples present the characteristic peaks of a fluorite-like cubic phase. No diffraction peaks of copper or manganese oxides are found in the diffraction patterns of the Cu- and Mn-doped samples. Table 1 summarizes the lattice constants of the samples. It is found that the doping of Mn induces the contraction of the cell volume of the ceria lattice, while the lattice constant of the Cu–Ce mixed oxides keeps unchanged. The ionic radii of Mn^{4+}, Mn^{3+}, Cu^{2+} and Cu^{+} are 0.56, 0.62, 0.73 and 0.77 Å, respectively, which are all smaller than that of Ce^{4+} (0.97 Å). The decrease in lattice constant of the Mn-doped ceria indicates the formation of MnO_x–CeO_2 solid solutions which have been widely verified in the literature [12,17,18]. On the other hand, the precise state of copper oxide in CuO_x–CeO_2 catalyst is still in debate [19]. Although substitution of Ce^{4+} by Cu^{+} at the interface of Cu–Ce was proposed [20], according to the similarity of lattice constants of Cu–Ce and CeO_2 in this paper, the copper oxides are more probably in the form of well dispersion or amorphous state in strong contact with the surface of ceria [21].

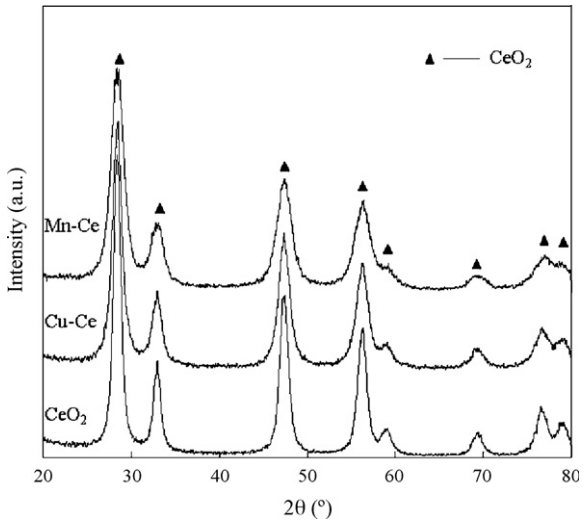

Fig. 1. XRD patterns of the samples.

Table 1 also lists the crystallite sizes of ceria-based oxides and specific surface areas of the samples. The crystallite sizes of the Cu–Ce and Mn–Ce obviously decrease compared with that of pure CeO_2, and their specific surface areas are correspondingly higher than that of ceria. These changes indicate that the textural structure of Cu–Ce and Mn–Ce is less affected by calcination than pure CeO_2. The introduction of transition metals, whether the surface enriched copper oxide or the incorporated manganese oxide, seems to restrict the growth of ceria crystallites and maintain the textural structure of the oxide sample. Higher specific surface area and smaller average crystallite size are favorable for the redox properties of the mixed oxides and activity for soot oxidation, which would be described in the following sections.

3.2. O_2-TPD

The oxygen desorption behaviors of the samples were investigated by O_2-TPD tests and the results are shown in Fig. 2. No obvious desorption peak is observed in the desorption profile of ceria in the experimental temperature range (100–800 °C), which correlates with the report [22] that the desorption peak of CeO_2 appears around 900 °C.

With the partial substitution of Ce by Mn, the desorption of O_2 is significantly enhanced. Two kinds of desorption peaks appear in the desorption profile of the Mn–Ce mixed oxides. The first one appearing in the range of 160–300 °C is ascribed to α-O_2 desorption and is related to molecular O_2, O_2^- and O_2^{2-} adsorbed on oxygen vacancies. The latter one in the range of 300–520 °C is designated as β-O_2 desorption and is attributed to the liberation of lattice oxygen from the oxides [23]. Since the Ce-substitution with di- or trivalent Mn ions produces oxygen vacancies in the fluorite-type lattice, the increased low-temperature desorption is associated with the oxygen vacancy [24]. Oxygen species of hydroxygen O_2^- and superoxygen O_2^{2-} can be formed by adsorbing O_2 at anion vacancy via reactions. (1) and (2) [25,26], which can be desorbed as α-O_2 during the test of O_2-TPD. The β-oxygen in the surface lattice of the Mn–Ce solid solutions can be desorbed from the temperature as low as 300 °C leading to the reduction of $Mn^{4+} \rightarrow Mn^{3+}$ and anion vacancy generation [18]. The β-O_2 desorption process continues via the diffusion of lattice oxygen from the bulk to the surface and the further reduction of $Mn^{3+} \rightarrow Mn^{2+}$ and $Ce^{4+} \rightarrow Ce^{3+}$. It confirms that the Mn incorporation enhances the mobility of lattice oxygen in ceria.

$$Ce^{3+}–V_{\ddot{O}}–Mn^{(n-1)+} + O_2 \leftrightarrow Ce^{4+}–O_2^-–Mn^{(n-1)+} \quad (1)$$

$$Ce^{4+}–O_2^-–Mn^{(n-1)+} \leftrightarrow Ce^{4+}–O_2^{2-}–Mn^{n+} \quad (2)$$

$$Ce^{3+}–V_{\ddot{O}}–Cu^{+} + O_2 \leftrightarrow Ce^{4+}–O_2^-–Cu^{+} \quad (3)$$

$$Ce^{4+}–O_2^-–Cu^{+} \leftrightarrow Ce^{4+}–O_2^{2-}–Cu^{2+} \quad (4)$$

No obvious α-O_2 desorption peaks are found in the O_2-TPD profile of the Cu–Ce mixed oxides. The minor peak around 675 °C may be induced via the reduction of Ce^{4+}–O^{2-}–Cu^{2+} pairs by similar equations as Eqs. (3) and (4), which only occur at the interface between copper oxide and ceria. A following intense β-O_2 desorption peak with a maximum at 780 °C is observed, which is ascribed to the lattice oxygen released via the reduction $Ce^{4+} \rightarrow Ce^{3+}$ and $Cu^{2+} \rightarrow Cu^{+} \rightarrow Cu^{0}$ [27]. It shows a drop in the desorption temperature with respect to pure ceria, suggesting the mobility of lattice oxygen is also improved via the doping of Cu. The cumulative area of desorption peak below 800 °C were integrated and the larger value of the Cu–Ce mixed oxides (1.7 mmol O_2/g cat.) compared with Mn–Ce (1.1 mmol O_2/g cat.) suggests a larger potential oxygen release capacity.

3.3. CO-TPR

It has been reported according to the H_2-TPR results that Cu- [28] and Mn- [29] doped ceria can be more easily reduced compared with the undoped one. In this work, the CO-TPR test was applied to evaluate the redox property of the samples. As shown in Fig. 3, only minor peaks are observed over CeO_2 in the temperature range from 300 to 450 °C, which are always due to the reduction of surface oxygen [28,30]. On the other hand, several intensified reduction peaks appear in the temperature range from 50 to 350 °C and from 100 to 550 °C for the Cu–Ce and Mn–Ce mixed oxides, respectively.

For the Mn–Ce mixed oxides, the reduction peaks around 150, 320 and 415 °C are obviously larger than those for pure CeO_2. Two types of oxygen species contribute to these peaks: one is the surface chemisorbed oxygen and the other comes from the reduction of $Mn^{4+} \rightarrow Mn^{3+}$, $Mn^{3+} \rightarrow Mn^{2+}$ and $Ce^{4+} \rightarrow Ce^{3+}$ [30]. The first one has a strong linkage with surface oxygen vacancies and it has been confirmed by O_2-TPD that a great amount of α-O_2

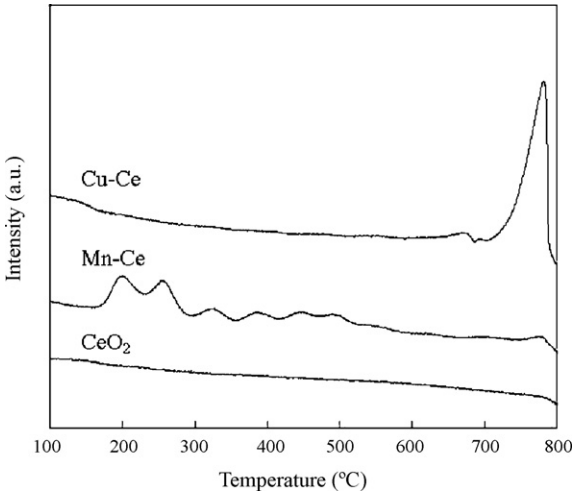

Fig. 2. O_2-TPD profiles of the samples.

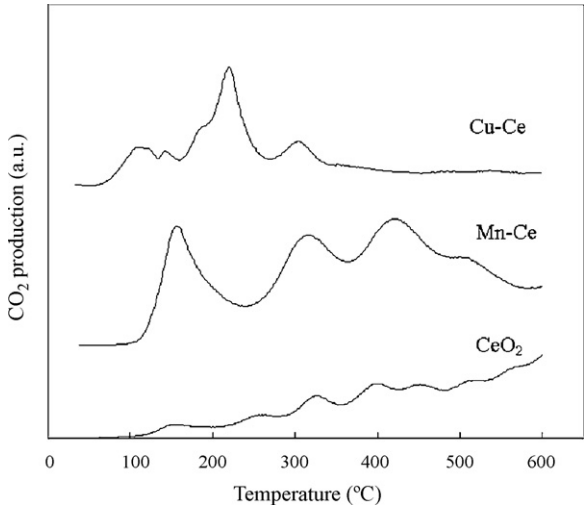

Fig. 3. CO-TPR profiles of the samples.

can be released from the Mn–Ce mixed oxides at low temperature. The formation of Mn–Ce solid solutions have a positive effect on the generation of surface oxygen vacancies from the low-valent Mn^{x+} ($x = 2, 3$) doping. Besides that, it is well demonstrated that the interaction between Mn and Ce in solid solutions heavily modifies the redox activity of manganese [31] and is good for the reduction of high-valent Mn^{x+} ($x = 3, 4$) to release oxygen.

Low-temperature reduction peaks are commonly observed in the H_2-TPR profile of the Cu–Ce mixed oxides, which are always attributed to highly dispersed CuO clusters strongly interacted with CeO_2. A similar phenomenon can be found when CO is used as the reduction agent. It is reported that two distinct peaks at ca. 225 and 320 °C are observed in the CO-TPR profile of CuO [32], which are also observed in the fresh Cu–Ce mixed oxides in the adjacent positions (220 and 305 °C) in our research. The formation of low-temperature peaks at ca. 110, 120 and 145 °C is remarkable in the system containing copper and ceria. Actually, a rapid increase of CO conversion is observed in this temperature range, suggesting that the most active sites for CO catalytic oxidation exist in the Cu–Ce interface with strong synergetic effect between these two elements.

3.4. Isothermal CO reduction

The oxygen release capacity of the samples under reducing condition was investigated via CO reduction tests at 300, 350, 400, 450 and 500 °C, respectively. The oxygen release capacity is defined as CO_2 produced per gram of the sample (mmol CO_2/g cat.) during the first 50 s of the test, and the results are shown in Table 2. Both the Cu–Ce and Mn–Ce mixed oxides show higher oxygen release capacities compared with pure ceria. The oxygen participating in CO oxidation should be released from the catalyst itself since the inlet gas did not contain any gaseous oxygen during the test. There are two types of oxygen species released from the catalyst. One is oxygen chemisorbed on the surface of the catalyst via adsorbing O_2 at anion vacancies during the oxidation pretreatment, which can be basically removed during the course of flushing by He with increasing the pretreating temperature. The other is the lattice oxygen from the surface or sub-surface of the catalyst, which is continuously complemented by the oxygen diffused from the bulk onto the surface. In this sense, the release capacity of lattice oxygen can be well presented by the results of CO reduction experiment, which follows the order of Cu–Ce > Mn–Ce > CeO_2. That is to say, the oxygen release capacity is always higher for Cu–Ce. It seems to be inconsistent with the O_2-TPD profiles in Fig. 2 that the oxygen desorption peaks appear from 160 and 675 °C for Mn–Ce and Cu–Ce in inert atmosphere, respectively. This difference should be mainly attributed to the reaction environment which plays a propulsive role for oxygen releasing. In other words, Cu–Ce mixed oxides are more easily to provide lattice oxygen in reducing atmosphere than Mn–Ce.

Based on the analysis of the structural features, most copper oxides exist in the form of well dispersion or amorphous state in strong contact with the surface of ceria. The interaction between Cu and Ce at Cu–Ce interface greatly improves the release ability of surface chemisorbed oxygen and lattice oxygen from the surface and sub-surface of oxides, which contributes the majority of the oxygen release capacity of the mixed oxides. Actually, it can be seen from the CO-TPR curve in Fig. 3 that the majority of oxygen is released from Cu–Ce before 300 °C. After then, the oxygen release capacity of Cu–Ce increases slowly with temperature. On the other hand, Mn–Ce maintains a steady increase in the oxygen release capacity with temperature as well as ceria, which is related the formation of solid solutions. By introducing manganese into ceria, the distortion of lattice structure and interaction between Mn and Ce enhance the mobility of lattice oxygen in the bulk, which increases with temperature as depicted in Fig. 3.

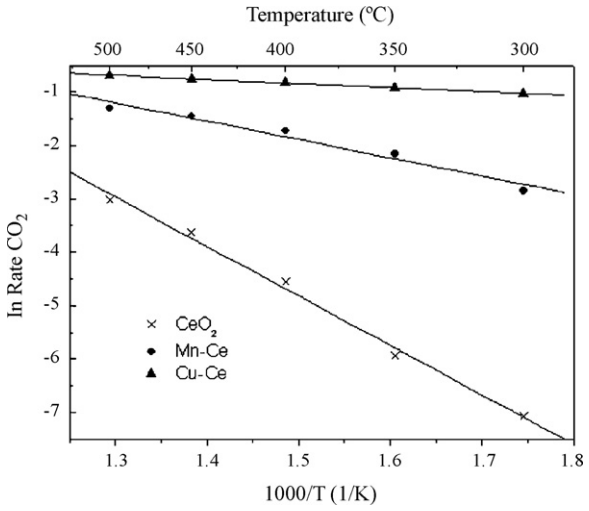

Fig. 4. Arrhenius plots for the samples when the Ce^{4+} reduction rate reached 6%.

The Arrhenius behavior of the samples was calculated by using the methods mentioned in Ref. [33] and the results are shown in Fig. 4. As suggested by Hori et al. [33], the CO_2 production rate at the slope was calculated according to the following equation:

$$\text{Rate } (\mu\text{mol CO}_2\,\text{g}^{-1}\,\text{s}^{-1}) = \frac{\int_{t_0}^{t_1} \text{CO}_2\text{signal}}{t_1 - t_0} \quad (5)$$

where t_1 was the time when the catalyst reached to 6% reduction of Ce^{4+} to Ce^{3+}, and t_0 was the starting time for the CO pulse, which always equaled to 0 s in our study. $\int_{t_0}^{t_1} CO_2$signal was the integrated peak area ranged from t_1 to t_0, and Rate (μmol CO_2 g^{-1} s^{-1}) was supposed to be the initial CO_2 production rate ranged from t_1 to t_0 since the time interval t_1–t_0 was short enough in this case. It also represents the average oxygen release rate, i.e. the lattice oxygen mobility in this case. It can be seen from Table 2 that doping with Cu or Mn not only increases the oxygen release capacity of ceria, but also promotes the lattice oxygen mobility, which follows the same order of Cu–Ce > Mn–Ce > CeO_2 especially at low temperatures.

The E_a of the catalyst was derived from the plots of ln Rate *vs.* 1/*T* according to Arrhenius equation Rate = A exp($-E_a/RT$), and the results are listed in Table 2. It is seen that the apparent activation energy for CO reduction is in the order of CeO_2 > Mn–Ce > Cu–Ce.

Table 2
The Arrhenius activation, oxygen release capacity and rate of the samples

Samples	E_a (kJ/mol)	Oxygen release capacity (mmol CO_2/g cat.)					Average oxygen release rate (mmol[O]/(g cat. s)				
		300 °C	350 °C	400 °C	450 °C	500 °C	300 °C	350 °C	400 °C	450 °C	500 °C
CeO_2	75	0.15	0.16	0.26	0.35	0.42	0.001	0.003	0.011	0.027	0.049
Cu–Ce	7	0.81	0.85	0.92	0.99	1.06	0.357	0.402	0.446	0.475	0.502
Mn–Ce	32	0.39	0.50	0.59	0.80	0.85	0.058	0.116	0.179	0.234	0.272

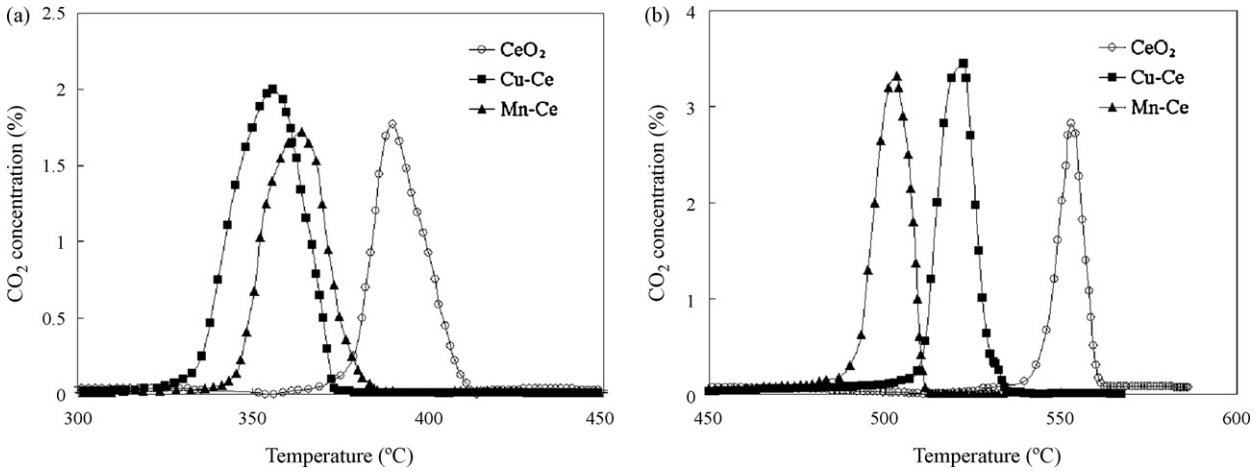

Fig. 5. TPO profile of Cu–Ce, Mn–Ce and CeO_2: (a) under tight contact conditions and (b) under loose contact conditions.

Considering the large amount of β-O_2 desorbed, the highest lattice oxygen release capacity and the lowest activation energy of CO reduction, Cu–Ce is supposed more readily to provide its lattice oxygen especially from the Cu–Ce interface [34,35].

3.5. Soot TPO

The activity of the catalysts for soot oxidation was evaluated under different catalyst–soot contact conditions and the results are shown in Fig. 5. It has been derived from [6] that the majority of soot could be converted by the catalyzed oxidation under tight contact conditions when the catalyst external surface area to the initial soot surface area ratio is above 0.4. In our experiment condition, the surface area ratio of catalyst to soot is above 0.6. Even there is multilayer of soot particles under loose contact conditions, with the pressure of high velocity flow air and the spillover effect of activated oxygen from gas by the catalyst, the majority of soot should be also catalytically oxidized. The temperature where the CO_2 concentration in the outlet gas reaches 0.5% is referred to as the ignition temperature (T_i) of soot oxidation, which in general reflects the intrinsic characteristics of the catalytic material and is relatively difficulty to be affected by reaction conditions. T_m represents the maximum oxidation rate temperature. The molar ratio of $CO_2/(CO_2 + CO)$ in the outlet gas is referred to as the selectivity to CO_2 (S) in the products. Table 3 lists the T_i, T_m, and $S(CO_2)$ of the catalysts for soot oxidation under different contact conditions. Both the mixed oxides show better soot oxidation activities than pure ceria. It is notable that the Mn–Ce mixed oxides show a better activity under loose contact conditions, while the Cu–Ce mixed oxides present some advantage under tight contact conditions. The selectivity to CO_2 production is similar over all the catalysts under tight contact conditions, while the CO_2 selectivity under loose contact conditions reaches 95% over the mixed oxides, indicating that the partial oxidation of soot is no longer a significant reaction compared with ceria. This improvement can be mainly ascribed to the high CO oxidation activity of manganese oxides [36] and copper oxides [28].

Table 3
Soot oxidation activity of the catalysts under different contact conditions

Samples	Tight contact			Loose contact		
	T_i (°C)	T_m (°C)	$S(CO_2)$ (%)	T_i (°C)	T_m (°C)	$S(CO_2)$ (%)
Mn–Ce	348	368	94	491	503	95
Cu–Ce	338	356	98	510	522	95
CeO_2	380	390	96	545	553	86

Obviously, the oxygen desorbed from the catalysts (1.7 and 1.1 mmol O_2/g cat. for Cu–Ce and Mn–Ce, respectively) is not enough to oxide all the soot. It should be noticed that this value was measured in an anaerobic atmosphere, while gaseous oxygen can continuously participate in the TPO reaction by filling the vacant sites on catalysts. As pointed out by Krishna et al. [6], the activation of oxygen and spill over of active oxygen from gas by the catalyst to soot particles are important intermediate steps in the soot oxidation mechanism [6]. The process of oxygen activation for Mn–Ce and Cu–Ce mixed oxides may occur at different sites according to the analyses of XRD and TPR. The active oxygen can be easily generated on the surface vacancies of Mn–Ce from chemisorbed oxygen while it is more likely to be produced on the Cu–O–Ce interface in Cu–Ce [13,37]. According to the results of O_2-TPD, great amounts of α- and β-O_2 can be desorbed from Mn–Ce mixed oxides at low temperature, which transfer from the catalyst to soot particle and act as active oxygen species via a spillover mechanism [16] and then are rapidly compensated from gaseous oxygen. The process is shown in Fig. 6a. In this way, the ignition temperature of soot oxidation for the Mn–Ce catalyst is the lowest under loose contact conditions.

The step which active oxygen species transfer from the catalyst to soot particle becomes relatively easier under tight contact conditions. Meanwhile, the supply of gaseous oxygen may become locally lacking during the reaction process in this case, which demands a strong lattice oxygen release ability of the catalyst. Although Cu–Ce and CeO_2 have similar O_2-TPD profiles in the soot combustion temperature range (below 600 °C) under inert atmosphere, the existence of Cu–Ce interface in Cu–Ce mixed oxides greatly facilitate the generation of active oxygen with the anticipation of reductant. It has been presented by the CO-TPR and isothermal CO reduction tests that oxygen species are more readily releasable from the Cu–Ce mixed oxides under reducing conditions, although the reductant becomes active carbon sites in soot oxidation. The surface and sub-surface lattice oxygen species in the Cu–Ce interface region are readily released, which are then rapidly complemented by gaseous oxygen and the lattice oxygen diffused from the vicinity of the interface. As a result, the Cu–Ce mixed oxides show the best activity under tight contact conditions due to the low activation energy of lattice oxygen release, as shown in Fig. 6b. Meanwhile, the Cu–Ce mixed oxides show the highest selectivity to CO_2 production, which is mainly ascribed to its superior CO oxidation activity [38].

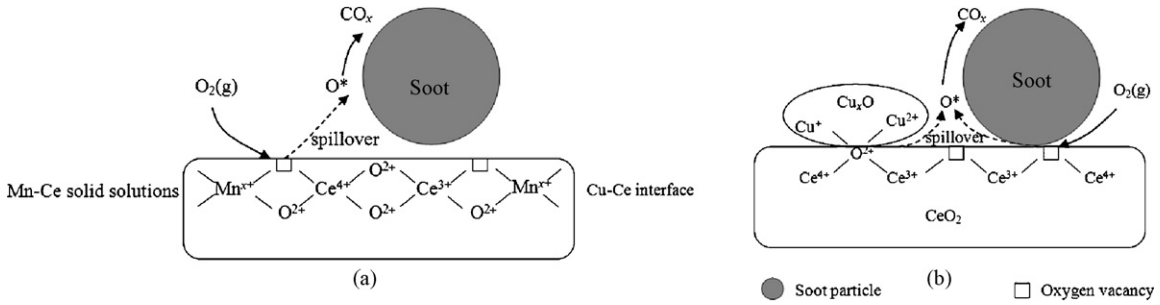

Fig. 6. Reaction mechanism and active oxygen species: (a) the Mn–Ce mixed oxides under loose contact conditions and (b) the Cu–Ce mixed oxides under tight contact conditions.

As described above, active oxygen that generates from chemisorbed oxygen on the surface vacancies of the Mn–Ce solid solutions has a significant effect under loose contact conditions, while that originates from readily releasable lattice oxygen in the Cu–Ce interface seems to be more important under tight contact conditions, After all, it should be noticed that these active oxygen species are both essential for soot oxidation under two contact conditions. The detailed dynamic process and specific roles of different oxygen species are still to be identified by using tools such as isotope exchange experiments.

4. Conclusions

Two different transition metals (Cu- or Mn-) doped ceria were synthesized by sol–gel method. MnO_x enters into the CeO_2 lattice to form the solid solutions, which generates more anionic vacancies to adsorb easily releasable α-O_2 on the surface and enhance the redox properties of the metal ions. Cu_xO clusters are highly dispersed on the surface of ceria particles, which induce a synergetic effect between these two elements and more readily releasable lattice oxygen. The difference of structural and morphology of the mixed oxides brings different soot oxidation behaviors under different contact conditions. By comparing study of these catalysts which generate active oxygen from different ways, it is proposed that surface oxygen vacancy and readily releasable lattice oxygen both play important roles in soot catalytic oxidation.

Acknowledgements

The authors would like to acknowledge the Ministry of Science and Technology of China which supported Projects 2004CB719503, 2006AA06Z346 and 2006AA060303.

References

[1] T. Masui, T. Ozaki, K. Machida, G. Adachi, J. Alloy Comp. 303–304 (2000) 49.
[2] C. Bozo, F. Gaillard, N. Guilhaume, Appl. Catal. A 220 (2001) 69.
[3] M.L. Pisarello, V. Milt, M.A. Peralta, C.A. Querini, E.E. Miró, Catal. Today 75 (2002) 465.
[4] A. Bueno-López, K. Krishna, M. Makkee, J.A. Moulijn, Catal. Lett. 99 (2005) 203.
[5] T. Masui, K. Minami, K. Koyabu, N. Imanaka, Catal. Today 117 (2006) 187.
[6] K. Krishna, A. Bueno-López, M. Makkee, J.A. Moulijn, Appl. Catal. B 75 (2007) 189.
[7] J. Liu, Z. Zhao, C. Xu, A. Duan, L. Wang, S. Zhang, Catal. Commun. 8 (2007) 220.
[8] J.F. Lamonier, S.P. Kulyova, E.A. Zhilinskaya, B.G. Kostyuk, V.V. Lunin, A. Aboukaïs, Kinet. Catal. 45 (2004) 429.
[9] J.F. Lamonier, S.P. Kulyova, V.V. Lunin, E.A. Zhilinskaya, A. Aboukaïs, J. Therm. Anal. Calorim. 75 (2004) 857.
[10] E. Aneggi, M. Boaro, C. de Leitenburg, G. Dolcetti, A. Trovarelli, J. Alloy Comp. 408–412 (2006) 1096.
[11] A. Bueno-López, K. Krishna, M. Makkee, J.A. Moulijn, J. Catal. 230 (2005) 237.
[12] K. Tikhomirov, O. Kröcher, M. Elsener, A. Wokaun, Appl. Catal. B 64 (2006) 72.
[13] Q. Liang, X. Wu, D. Weng, Z. Lu, Catal. Commun. 9 (2008) 202.
[14] X. Wu, Q. Liang, D. Weng, Z. Lu, Catal. Commun. 8 (2007) 2110.
[15] J.P.A. Neeft, M. Makkee, J.A. Moulijn, Fuel Proc. Technol. 47 (1996) 1.
[16] B.A.A.L. van Setten, M. Makkee, J.A. Moulijn, Catal. Rev. Sci. Eng. 43 (2001) 489.
[17] G. Qi, R.T. Yang, R. Changb, Appl. Catal. B 51 (2004) 93.
[18] M. Machida, M. Uto, D. Kurogi, T. Kijima, Chem. Mater. 12 (2000) 3158.
[19] G. Avgouropoulos, T. Ioannides, H. Matralis, Appl. Catal. B 56 (2005) 87.
[20] S. Hocevar, U.O. Krasovec, B. Orel, A.S. Arico, H. Kim, Appl. Catal. B 28 (2000) 113.
[21] P. Bera, K.R. Priolkar, P.R. Sarode, M.S. Hegde, S. Emura, R. Kumashiro, N.P. Lalla, Chem. Mater. 14 (2002) 3591.
[22] D. Fino, V. Specchia, Chem. Eng. Sci. 59 (2004) 4825.
[23] S. Kaliaguine, A. van Neste, V. Szabo, J.E. Gallot, M. Bassir, R. Muzychuk, Appl. Catal. A 209 (2001) 345.
[24] M. Machida, Catal. Surv. Jpn. 5 (2002) 91.
[25] R. Zhang, A. Villanueva, H. Alamdari, S. Kaliaguine, J. Mol. Catal. A 258 (2006) 22.
[26] H. Chen, A. Sayari, A. Adnot, F. Larachi, Appl. Catal. B 32 (2001) 195.
[27] R. Zhou, T. Yu, X. Jiang, F. Chen, Appl. Surf. Sci. 148 (1999) 148.
[28] X. Tang, B. Zhang, Y. Li, Y. Xu, Q. Xin, W. Shen, Appl. Catal. A 288 (2005) 116.
[29] M. Machida, D. Kurogi, T. Kijima, Chem. Mater. 12 (2000) 3165.
[30] G. Picasso, M. Gutiérrez, M.P. Pina, J. Herguido, Chem. Eng. J. 126 (2007) 119.
[31] S. Imamura, M. Shono, N. Okamoto, A. Hamada, S. Ishida, Appl. Catal. A 142 (1996) 279.
[32] J.W. Park, J.H. Jeong, W.L. Yoon, C.S. Kim, D.K. Lee, Y.K. Park, Y.W. Rhee, Int. J. Hydrogen Energy. 30 (2005) 217.
[33] C.E. Hori, A. Brennera, K.Y. Simon Ng, K.M. Rahmoeller, D. Belton, Catal. Today 50 (1999) 299.
[34] G. Marbán, A.B. Fuertes, Appl. Catal. B 57 (2005) 43.
[35] A. Pintar, J. Batista, S. H?cevar, J. Colloid Interface Sci. 307 (2007) 145.
[36] S. Cimino, S. Colonna, S. De Rossic, M. Faticantic, L. Lisid, I. Pettitic, P. Porta, J. Catal. 205 (2002) 309.
[37] A. Martínez-Arias, M. Fernández-García, O. Gálvez, J.M. Coronado, J.A. Anderson, J.C. Conesa, J. Soria, G. Munuera, J. Catal. 195 (2000) 207.
[38] G. Avgouropoulos, T. Ioannides, Appl. Catal. B 67 (2006) 1.